HHS Public Access

Author manuscript

Nat Neurosci. Author manuscript; available in PMC 2018 October 09.

Published in final edited form as:

Nat Neurosci. 2018 May ; 21(5): 717–724. doi:10.1038/s41593-018-0126-0.

A hypothalamic circuit for the circadian control of aggression

William D. Todd[1,±], **Henning Fenselau**[2,±], **Joshua L. Wang**[1], **Rong Zhang**[3], **Natalia L. Machado**[1,4], **Anne Venner**[1], **Rebecca Y. Broadhurst**[1], **Satvinder Kaur**[1], **Timothy Lynagh**[5], **David P. Olson**[6], **Bradford B. Lowell**[2], **Patrick M. Fuller**[1], and **Clifford B. Saper**[1,*]

[1]Department of Neurology, Program in Neuroscience, Beth Israel Deaconess Medical Center and Harvard Medical School, Boston, Massachusetts, 02215, USA

[2]Division of Endocrinology, Diabetes and Metabolism, Department of Medicine, Program in Neuroscience, Beth Israel Deaconess Medical Center, Harvard Medical School, Boston, MA, USA, 02215

[3]Division of Endocrinology, Boston Children's Hospital and Harvard Medical School, Boston, Massachusetts, 02215, USA

[4]Department of Physiology and Biophysics, Federal University of Minas Gerais, Belo Horizonte-MG 31270-901, Brazil

[5]Department of Drug Design and Pharmacology, University of Copenhagen, Copenhagen, Denmark

[6]Department of Pediatrics, University of Michigan, Ann Arbor, MI 48109, USA

Abstract

"Sundowning" in dementia and Alzheimer's disease is characterized by early evening agitation and aggression. While such periodicity suggests a circadian origin, whether the circadian clock directly regulates aggressive behavior is unknown. We demonstrate that a daily rhythm in aggression propensity in male mice is gated by GABAergic subparaventricular zone (SPZ^{GABA}) neurons, the major postsynaptic targets of the central circadian clock, the suprachiasmatic nucleus (SCN). Optogenetic mapping revealed that SPZ^{GABA} neurons receive input from vasoactive intestinal polypeptide SCN neurons and innervate neurons in the ventrolateral part of the ventromedial hypothalamus (VMHvl) known to regulate aggression. Additionally, VMH-projecting dorsal SPZ neurons are more active during early day than early night, and acute chemogenetic inhibition of SPZ^{GABA} transmission phase-dependently increases aggression. Finally, SPZ^{GABA}-recipient central VMH neurons directly innervate VMHvl neurons and

*corresponding author. Contact: Clifford B. Saper, M.D., Ph. D., Beth Israel Deaconess Medical Center, Department of Neurology, 330 Brookline Ave, Boston, MA 02215, Phone: 617-667-2622, csaper@bidmc.harvard.edu.

±equal contribution

Author Contributions

W.D.T, H.F., and C.B.S. designed the experiments. W.D.T., H.F., J.L.W., R.Z., and N.L.M. carried out these experiments. J.L.W., A.V., S.K., T.L., D.P.O, B.B.L. and P.M.F. provided analytic tools and reagents. W.D.T., H.F., J.L.W., R.Z., A.V., and K.Y.B. analyzed the data. W.D.T, H.F., P.M.F, and C.B.S. wrote the paper.

Competing Financial Interests

The authors declare no competing financial interests.

activation of this intra-VMH circuit drove attack behavior. Altogether, we reveal a functional polysynaptic circuit by which the SCN clock regulates aggression.

Circadian rhythm disruption is a prominent feature of numerous neurodegenerative, neurodevelopmental, and neuropsychiatric diseases that are also associated with verbal and physical aggression[1–5]. However, whether the central circadian clock directly regulates aggression, a complex motivated behavior[6–10], and the circuit basis by which it may do so, remain unknown. We hypothesized that the propensity towards aggressive behavior varies across the 24 h day, and that the central circadian clock, located in the suprachiasmatic nucleus of the hypothalamus (SCN)[11], regulates this rhythm in aggression propensity. Neurons within the ventrolateral part of the ventromedial nucleus of the hypothalamus (VMHvl) are known to directly regulate attack behavior in male mice[10,12–15], but it is unknown if the activity of these neurons is under temporal regulation by the SCN clock. SCN neurons can function as individual oscillators exhibiting rhythmic electrical activity with a period of about 24 h[16], and this rhythmic activity is controlled by an internal transcriptional-translational-postranslational feedback loop under the control of canonical clock genes[11,17]. While this same genetic machinery is present in cells throughout the body, the SCN is necessary to synchronize peripheral oscillators and maintain rhythmic behavior, and axonal output appears to be the primary method by which the SCN establishes such synchrony *in vivo*[18,19]. Therefore, we hypothesized that the circadian regulation of aggression may depend upon a polysynaptic pathway from the SCN to VMHvl neurons.

We tested this hypothesis using optogenetically-based circuit mapping and a series of genetically-targeted neuronal manipulations with an initial focus on the GABAergic subparaventricular zone (SPZ^{GABA}), an obligate relay for most SCN clock synaptic output[19–22]. Our work reveals that aggression propensity exhibits a robust daily rhythm and that a circuit, spanning four synaptically coupled hypothalamic nodes, directly modulates this daily rhythm of aggression, primarily by inhibiting aggressive behavior in a circadian phase-dependent manner.

RESULTS

Aggression propensity exhibits a daily rhythm mediated by SPZ^{GABA} transmission

We first sought to examine whether the propensity for behavioral aggression follows a daily rhythm in mice and, if so, whether disabling neurotransmission by the SPZ, the major synaptic relay between the SCN clock and downstream structures[19–22], would disrupt this rhythm. We operationally defined the SPZ (Fig. 1a) as the region innervated by axons of vasoactive intestinal polypeptide (VIP) SCN neurons (SCN^{VIP}) and bordered ventrally and dorsally by arginine vasopression (AVP) neurons of the SCN and the paraventricular nucleus (PV), respectively, which is consistent with previous definitions in other rodent species[21–23]. Given that the SPZ is predominantly GABAergic, we used transgenic mice expressing loxP sites flanking the second exon of *Vgat, Slc32a1*, the gene for the vesicular GABA transporter (VGAT, $Vgat^{lox/lox}$ mice)[24]. By placing injections of an adeno-associated viral vector (AAV) containing Cre recombinase (AAV-iCre-2A-Venus)[25] into the SPZ (Fig. S1), we deleted this gene (Fig. S2), rendering SPZ cells unable to release GABA. We specifically

targeted these injections towards the dorsal SPZ (dSPZ), as this region has been shown to predominately target the VMH in rats[23]. We then tested SPZ *Vgat*-deleted mice and their intact littermates (injected with AAV-GFP into the SPZ, which does not delete *Vgat*), using the resident intruder paradigm (a well-established assay for territorial aggression in male mice)[6,10,12,14], at zeitgeber times (ZT)1, ZT7, ZT13, and ZT19 (ZT0=lights-on, 12/12 light-dark cycle).

We found that aggression propensity in intact male mice toward a male mouse intruder exhibited a daily rhythm with the highest total time spent engaged in attack behavior at ZT13 and the lowest at ZT1 (ZT13: 62.16 ± 12.52, ZT1: 24.95 ± 7.29, P=0.0067, Fig. 1b, blue). Intact GFP-injected mice also exhibited the highest number of attacks at ZT13 and the lowest number at ZT1 (ZT13: 19.38 ± 3.72, ZT1: 8.75 ± 2.30, P=0.0244, Fig. 1c, blue). This aggression propensity rhythm was completely lost in SPZ *Vgat*-deleted mice (number of attacks, ZT13: 18.63 ± 4.37, ZT1: 16.38 ± 2.21, P=0.99, Fig. 1c, red), and was accompanied by a significant increase in total time attacking at ZT1 compared to intact GFP-injected controls (deleted: 65.98 ± 8.13, intact: 24.94 ± 7.29, P=0.0055, Fig. 1b, red). Additionally, we found that attack latency was significantly affected (time X condition interaction, P=0.0362), with intact GFP-injected mice exhibiting a trend towards lower latencies at ZT13 compared to ZT1 (ZT13: 158.26 ± 41.32, ZT1: 284.26 ± 57.81, P=0.0605, Fig. 1d, blue), and SPZ *Vgat*-deleted mice exhibiting a trend towards decreased latency to attack at ZT1 compared to intact GFP-injected controls (deleted: 142.34 ± 22.95, intact: 284.26 ± 57.81, P=0.0683, Fig. 1d, red). Importantly, we also found that the lower propensity for aggression during the early resting phase in intact mice was not simply due to the direct effects of light. Specifically, control mice tested under free running conditions in constant darkness (DD) showed similar temporal differences in total time attacking between early subjective day and early subjective night [circadian time (CT)1: 12.47 ± 7.38, CT13: 27.30 ± 8.23, P=0.0305, Fig. S3], suggesting these rhythms are circadian in nature.

SPZ *Vgat* deletions also reduced the amplitude of entrained (under a 12–12 light-dark cycle, LD) and free running (in DD) rhythms of locomotor activity (LMA, Table 1 and Fig. 1f–g), as well as the difference in day-night levels of plasma corticosterone (Fig. 1h). Specifically, in LD conditions, SPZ *Vgat* deletions significantly blunted the elevated LMA counts observed in control mice during the dark period (Fig. 1g), strongly so at ZT12 (deleted: 4.64 ± 0.66, intact: 7.84 ± 0.86), ZT13 (deleted: 4.61 ± 0.66, intact: 8.48 ± 2.13), and ZT23 (deleted: 3.48 ± 0.47, intact: 6.98 ± 1.53). Blunted elevation of plasma corticosterone levels at ZT13 as compared to controls was also observed (deleted: 13.82 ± 4.54, intact: 29.24 ± 8.31). Importantly, SPZ *Vgat* deletions did *not* significantly increase LMA counts (deleted: 1.24 ± 0.24, intact: 1.43 ± 0.26) or plasma corticosterone (deleted: 2.61 ± 0.72, intact: 1.98 ± 0.62) during the early light period (ZT1) when peak changes in attack behavior were observed, suggesting that the SPZ mediation of aggression propensity is independently regulated from LMA and plasma corticosterone rhythms. We should note that, although in some mice AAV-iCre-2A-Venus transduced cells in the PV (Fig. 1e), a structure extensively implicated in corticosterone regulation[26], the mouse PV contains relatively few *Vgat*[27] neurons and hence its function was unlikely to be affected by Cre injections. Interestingly, we did not find any differences in entrained or free-running rhythms of body temperature

(Tb, Table 1 and Fig. S4), which is consistent with previous work demonstrating the dissociability of individual circadian rhythms[28].

SPZ^{GABA} neurons inhibit VMH neurons and receive input from SCN^{VIP} neurons

Given that the SPZ functions largely as a post-synaptic relay for the circadian clock[19,20,22], we sought to define the functional synaptic circuitry by which the SPZ may control daily rhythms of aggression. We first asked whether SPZ^{GABA} neurons have functional synaptic connections with neurons of the VMH (Fig. 2a), a hypothalamic region known to regulate attack behavior[10,12–15]. To do this, we placed stereotaxically-guided injections of an AAV containing the gene for Cre-dependent expression of channelrhodopsin (ChR2, AAV-DIO-ChR2-mCherry) into the SPZ of mice engineered to express Cre in VGAT+ cells (*Vgat*-IRES-Cre mice)[27]. We then optogenetically mapped projections from SPZ^{GABA} neurons (Fig. 2b) by recording light-evoked inhibitory postsynaptic currents (IPSCs) from randomly selected VMH neurons (ChR2 assisted circuit mapping, or CRACM)[29,30]. We detected light-evoked IPSCs, which were completely abolished by the $GABA_AR$ antagonist bicuculline, in almost all (25 of 28) VMH neurons, confirming functional synaptic connectivity between SPZ^{GABA} and VMH neurons. We next sought to establish functional synaptic connectivity between SCN^{VIP} and VMH-projecting SPZ^{GABA} neurons ($SPZ^{\rightarrow VMH}$; Fig. 2c). To do this, we placed stereotaxic injections of a Cre-dependent ChR2 fused with EYFP (AAV-DIO-ChR2-EYFP) into the SCN of *VIP*-IRES-Cre[31] mice and a fluorescent retrograde tracer (CTb-555) into the VMH (to label $SPZ^{\rightarrow VMH}$ neurons) of the same mice. We detected light-evoked GABAergic IPSCs in the majority of $SPZ^{\rightarrow VMH}$ neurons (5 of 9), confirming functional synaptic connectivity between SCN^{VIP} and SPZ^{GABA} neurons that project to the VMH. Our CRACM results therefore show that SCN^{VIP} neurons provide GABAergic input to SPZ neurons that innervate the VMH and that SPZ^{GABA} neurons subsequently inhibit the VMH. This pathway provides a possible circuit substrate by which the SCN may modulate the activity of VMH neurons, including VMH neurons that regulate aggression.

To obtain a more detailed anatomic understanding of the $SPZ^{GABA}\rightarrow$VMH pathway, we injected an AAV coding for Cre-dependent expression of the anterograde tracer humanized *Renilla* Green Fluorescent Protein (AAV-FLEX-hrGFP) into the SPZ of *Vgat*-IRES-Cre mice (Fig. 2d–f). Consistent with the foregoing optogenetic mapping experiments, we found that SPZ^{GABA} neurons densely innervate the central VMH (VMHc), and to a lesser extent the dorsomedial VMH (VMHdm) and ventrolateral VMH (VMHvl). Using subtraction methods across mice with different hrGFP injection sites, we found that VGAT+ neurons within the dSPZ predominately target the VMH, whereas VGAT+ neurons within the more ventral portions of the SPZ predominately target the DMH (Fig. S5). A similar topographic organization of SPZ projections was previously reported in rats[23]. When we constructed a heat map showing the regions of the SPZ in which *Vgat*-deletion produced maximal disruption of rhythms of aggression, the most critical region included the dSPZ, which maximally innervates the VMH (Fig. 1e). Importantly, we also noted that SPZ^{GABA} projections show ramification and dense synaptic boutons among estrogen receptor 1 (Esr1)-expressing neurons within the VMHvl (Fig. 2f), which have previously been shown to regulate attack behavior in male mice[12,14]. To examine whether SPZ projections to these cells form GABAergic synaptic connections we performed CRACM experiments using

Esr1-2a-Cre mice[14]. Toward this end, Cre-independent ChR2 (AAV-CAG-ChR2-mCherry) was targeted to SPZ neurons and Esr1-expressing neurons were transduced with AAV-FLEX-hrGFP for their identification in brain slices (Fig. 2g). We detected light-evoked IPSCs, which were completely abolished by the $GABA_AR$ antagonist bicuculline, in 10 out of 10 Esr1-expressing neurons, confirming direct functional synaptic connectivity between the SPZ neurons (which are nearly all GABAergic) and the VMHvl aggression locus.

Dorsal $SPZ^{\rightarrow VMH}$ neurons are active at ZT1 and acutely inhibiting them increases aggression

To determine whether low levels of aggressive behavior at ZT1 are associated with increased activity of $SPZ^{\rightarrow VMH}$ neurons, we examined expression of Fos, a marker of neuronal excitation. First, we perfused control mice 90 min after ZT1 and found a high number of Fos-labeled cells in the dSPZ (Fig. S6). Using retrograde tracing with CTb, we next showed that these dSPZ neurons specifically project to the VMH (Fig. 3a), and are significantly more active at ZT1 compared to ZT13 (Fig. 3b–c; $t_{(16)}$=3.903, P=0.0013), altogether suggesting that low levels of aggression at ZT1 are gated by this $dSPZ^{\rightarrow VMH}$ pathway.

Next, we examined the effects of acutely disrupting SPZ activity on aggression at ZT1 compared to ZT13. To inhibit SPZ neurons, we used a newly developed inhibitory viral vector that employs a mutated human glycine receptor in a Cre-dependent configuration (AAV-FLEX-hGlyR-mCherry; hGlyR-AAV, Fig. 3d). The hGlyR receptor is mutated to respond to the antiparasitic drug ivermectin (IVM), instead of its normal ligand glycine[32]. We placed small bilateral injections of the hGlyR-AAV into the SPZ of *Vgat*-IRES-Cre mice and then tested the effects of acute inhibition of SPZ^{GABA} neurons on aggression at either ZT1 or ZT13. At ZT1, mice showed significantly higher total time attacking [Fig. 3e, left; $t_{(7)}$=4.404, P=0.0031], higher number of attacks [Fig. 3e, center; $t_{(7)}$=4.615, P=0.0024], and lower attack latencies [Fig. 3e, right; $t_{(7)}$=5.686, Ps=0.0007] after the administration of IVM (5 mg/kg in propylene glycol) compared to vehicle (VEH). In contrast, at ZT13, IVM did not significantly change the total time attacking [Fig. 3f, left; $t_{(7)}$=0.5467, P=0.6016], number of attacks [Fig. 3f, center; $t_{(7)}$=1.93, P=0.0949], or attack latency [Fig. 3f, right; $t_{(7)}$=1.118, P=0.3005] compared to VEH. We also found that this effect was not due to a phase-dependent effect of IVM at ZT1, as control animals did not show increased aggression compared to VEH conditions at this time (Fig. S7).

To verify that the hGlyR-AAV and IVM inhibited SPZ^{GABA} neurons, we examined Fos expression in the dSPZ (which was among the most heavily weighted areas in the heat maps of our injection sites, Fig. 3i). Importantly, we found that *Vgat*-IRES-Cre mice injected with hGlyR-AAV in the SPZ and receiving IVM showed a significant decrease in the number of cFos expressing cells at ZT1 in the dSPZ compared to mice receiving VEH [Fig. 3i–j; $t_{(4)}$=3.497, P=0.025], indicating that hGlyR-AAV and IVM successfully inhibited $dSPZ^{GABA}$ neurons. Although *Vgat*-IRES-Cre mice as a substrain were less aggressive overall than $Vgat^{lox/lox}$ mice, the acute, reversible neuronal inhibition permitted a within-animal design, which improved the sensitivity of the aggression assay, and demonstrated that inhibition of dSPZ neurons increased aggression at ZT1, recapitulating the results following chronic disruption of SPZ^{GABA} neurotransmission.

An intra-VMH circuit receives circadian input and drives aggression

While SPZ^{GABA} neurons project directly to VMHvl neurons, our mapping experiments show that SPZ^{GABA} neurons most densely innervate the VMHc (Fig. 2 and Fig. S5). Therefore, we asked whether VMHc neurons engage and consequently excite VMHvl neurons, which then drive aggressive behavior (Fig. 4a), since the vast majority of VMH neurons are glutamatergic (VGLUT2-expressing)[27] and hence excitatory. Importantly, such a SCN→SPZ→VMHc→VMHvl circuit could thus form a parallel pathway that also regulates daily rhythms of aggression propensity. To investigate this possibilty, we used *Pacap*-IRES-Cre mice (PACAP, peptide pituitary adenylate cyclase activation polypeptide), which express *Pacap* (*Adcyap1*), and hence Cre-recombinase, in many VMHc neurons, but in much fewer VMHdm or VMHvl neurons[29]. We first assessed axonal projections of PACAP neurons in the VMHc ($VMHc^{PACAP}$ neurons) by stereotaxically injecting the anterograde tracer AAV-DIO-Synaptophysin-mCherry into the VMHc of *Pacap*-IRES-Cre mice. We found that both the VMHc and the VMHvl contained many $VMHc^{PACAP}$ terminals (Fig. 4b). In contrast, we found only a few $VMHc^{PACAP}$ terminals in the VMHdm (Fig. 4b).

We next ascertained functional synaptic connectivity between $VMHc^{PACAP}$ and VMHdm, VMHc, or VMHvl neurons using CRACM (Fig. 4c). For this, we placed injections of AAV-DIO-ChR2-mCherry into the VMHc of *Pacap*-IRES-Cre mice and recorded light-evoked excitatory postsynaptic currents (EPSCs) from ChR2/mCherry-negative neurons (Fig. 4c). Consistent with the tracing data, we detected light-evoked EPSCs in almost all VMHc and VMHvl neurons (13 out of 15 neurons; Fig. 4c). In contrast, we detected light-evoked EPSCs in only 1 out of 13 VMHdm neurons (Fig. 4c). Thus $VMHc^{PACAP}$ neurons densely innervate and excite VMHc and VMHvl neurons, but not VMHdm neurons.

To determine if acute stimulation of $VMHc^{PACAP}$ neurons drives behavioral aggression, we placed bilateral injections of Cre-dependent excitatory chemoreceptor (AAV-DIO-hM3Dq-mCherry; hM3Dq) into the VMHc of *Pacap*-IRES-Cre mice (Fig. 4d). Administration of the hM3Dq ligand, clozapine-N-oxide (CNO, 1 mg/kg in saline), significantly increased total time attacking compared to VEH [Fig. 4e; $t_{(5)}=3.337$, $P=0.0206$]. Strong induction of cFos served as further confirmation that CNO effectively activated $VMHc^{PACAP}$ neurons (Fig. 4f). In agreement with our tracing and CRACM experiments, acute activation of $VMHc^{PACAP}$ neurons also increased cFos expression in VMHvl neurons, strongly suggesting that the increase in aggression was driven by this intra-VMH connection.

DISCUSSION

Here we demonstrate, for the first time, that aggression propensity in male mice exhibits a daily rhythm. We then show using genetically targeted disruption and inhibition that this rhythm in aggression propensity requires normal functioning of SPZ^{GABA} neurons and is independent of LMA and plasma corticosterone rhythms. Using the CRACM approach[29,30], we uncover a novel and functional polysynaptic circuit connecting the SCN clock with VMHvl neurons known to regulate attack behavior. We also show a parallel pathway from the SPZ through PACAP-expressing neurons within the VMHc that are highly

interconnected with the VMHvl, forming an intra-VMH circuit that, upon activation, also drives attack behavior.

Agonistic encounters between conspecific males are characterized by the progression from an investigative motivational phase[33], in which the sex, size, and strength of the opponent are determined, to a consummatory phase comprised of attack behavior or retreat[7], and this progression is generally conceptualized as an escalation in the intensity of a continuous internal emotional state[34,35]. Our data strongly suggest that input from the SCN clock to VMHvl neurons, either directly from SPZ neurons or indirectly through VMHc neurons, may increase or decrease the rate of this progression and the intensity or duration of consummatory attack behavior depending on the time of day of the encounter. Indeed, because the VMHc has also been shown to be relevant in other emotionally related behaviors associated with fear and anxiety[36,37], it is possible that this novel circuit may modulate circadian rhythms in the propensity for such behaviors as well[38,39].

Since SCN activity in mice is high during the day and less active at night[40], it is interesting that dSPZ$^{\rightarrow VMH}$ neurons, which receive GABAergic input from the SCN (Fig. 2a–c) are more active at ZT1 compared to ZT13 (Fig. 3a–c). We therefore believe that it is the summation of inhibitory GABAergic SCN→dSPZ input across the day that leads to low levels of dSPZ→VMH inhibiton, and therefore increased aggression propensity, during the end of the light and the early dark period (CT11 and 13, Fig. S3; ZT13, Fig. 1b–d). Furthermore, we believe the reduction of SCN activity during the night allows for the summation of GABAergic dSPZ→VMH inhibition over the dark period, leading to the lowest aggression propensity during the early light period (ZT1). A previous study examining SCN and SPZ multiunit activity (MUA) in mice reported that SPZ MUA was highest during the dark period[40], antiphase to the day-active SCN, however the recording sites depicted in a supplementary figure for that paper appear to be rostral and ventral to the dSPZ region which we show is highly active at ZT1. The SPZ is known to be composed of multiple subregions with differing input and output pathways[23], and which appear to modulate dissociable circadian rhythms[22]. Thus, the temporal pattern of activity for each SPZ subregion may be influenced by several other factors, such as intra-SPZ connectivity from other subregions[23], direct input from the retina[41], peptidergic input from different subpopulations within the SCN (VIP, AVP, etc.)[42], as well as input from other neural systems. Regardless of the underlying cause of increased dSPZ activity at ZT1, our results demonstrate that GABAergic transmission from these neurons serves to inhibit the propensity for aggression during the early resting period, most likely via their projections to the VMH.

A better understanding of how the SCN clock and its primary synaptic relay, the SPZ, modulate aggressive behavior will have important implications for treating patients with neurological disorders associated with circadian dysfunction and physical and verbal aggression. For instance, patients suffering from dementia and Alzheimer's disease frequently exhibit sundowning syndrome[2,43–45], a poorly understood clinical phenomenon characterized by agitation, aggression, and delirium during the early evening hours. These symptoms take a tremendous toll on the patient's caregivers and represent a common reason for institutionalization[46]. Our results showing that disruption of SPZ^{GABA} output produces

increased behavioral aggression during the early resting phase (morning for mice) are temporally consistent with the increased aggression seen during sundowning, suggesting that the SCN→SPZ→VMH pathway may be compromised in such neurodegenerative diseases. An examination of neuropathological changes to this pathway in AD and other neurological conditions may provide insight into future interventions that could greatly improve the quality of life for both patients and caregivers.

ONLINE METHODS

Animals

Adult male *Vgat*$^{lox/lox}$, *Vgat*-IRES-Cre, *VIP*-IRES-Cre, *Esr1*-2a-Cre, *Pacap*-IRES-Cre, and C57BL6/J mice were used. *Vgat*$^{lox/lox}$ mice, *Vgat*-IRES-Cre mice, *VIP*-ires-Cre and Pacap-IRES-Cre mice were described previously[24,27,29,31]. *Esr1*-2a-Cre mice were obtained from Jackson laboratories (Stock No: 017911). *Vgat*-IRES-Cre and *Vgat*$^{lox/lox}$ lines had been backcrossed to the C57BL6/J strain, whereas *Pacap*-IRES-Cre mice were mixed background. C57BL6/J mice were obtained from Jackson Laboratories. All procedures were performed in accordance with the National Institutes of Health Guide for the Care and Use of Laboratory Animals, and formal approval of our protocols was obtained from the Institutionary Animal Care and Use Committee at Beth Israel Deaconess Medical Center. All efforts were made to minimize pain and the number of mice used. Additional information about the following procedures can be found in the Life Sciences Reporting Summary for this paper.

AAV-FLEX-hGlyR-mCherry generation

We used a human alpha-1 glycine receptor gene, modified by Lynagh and Lynch and previously tested in vitro[32], in which A288G and F207A mutations were induced to render the channel almost 100 times more sensitive to the antiparasitic IVM, but insensitive to glycine. This construct was placed within a DIO/FLEX cassette and packaged within an AAV, serotype 10 by Dr. Patrick Fuller.

Other vectors used

AAV-iCre-2A-Venus contains genes for Cre and Venus, a GFP, connected via a self-processing 2A viral peptide bridge[25]. Plasmid construct was donated by Dr. Rolf Sprengel from the University of Heidelberg, Germany, cloned and sequenced in our laboratory, and packaged by Dr. Jeng-Shin Lee, Harvard Gene Therapy Initiative, in AAV (serotype 8; titer=9.4×10^{12} GC/ml). AAV-DiO-ChR2-mCherry-WPRE (serotype 8; titer=3.8×10^{12} GC/ml) was produced at the University of North Carolina virus core from plasmid provided by Dr. Karl Deisseroth from Stanford University, Palo Alto, CA. AAV9-FLEX-ChR2(H134R)-EYFP was obtained from University of Pennsylvania School of Medicine. Cholera Toxin Subunit B (Recombinant), Alexa Fluor® 555 Conjugate was obtained from Thermo Fisher (C-34776). AAV-FLEX-hrGFP was provided by Drs. Patrick Fuller and Michael Lazarus. AAV8-DIO-hM3Dq-mCherry was obtained from the University of North Carolina Vector Core. AAV8-DIO-synaptophysin-mCherry was obtained from Virovek, Inc.

Surgeries

Mice were anesthetized with ketamine/xylazine [100 and 10 mg/kg respectively, intraperitoneally (IP)] and placed in a stereotaxic apparatus. Injections were placed into SPZ (AP=−0.4 mm, ML=±0.2 mm, DV=−5.1 mm), SCN (AP=−0.4 mm, ML=±0.1 mm, DV=−5.5 mm), or VMH (AP=−1.6 mm, ML=±0.5 mm, DV=−5.6 mm) using a compressed air delivery system. AAV-FLEX-hrGFP or AAV-DiO-ChR2-mCherry (10–15 nl) was injected unilaterally into the SPZ of *Vgat*-IRES-Cre mice. AAV-FLEX-hGlyR-mCherry (30 nl) was injected bilaterally into the SPZ of *Vgat*-IRES-Cre mice. AAV-DIO-ChR2-EYFP (~60 nl) and CTb-555 (~5 nl) were injected unilaterally into the SCN and VMH, respectively, of *VIP*-IRES-Cre mice. AAV-CAG-ChR2-mCherry (10 nl) and AAV-FLEX-hrGFP (30 nl) were injected into the SPZ and VMH of *Esr1*-2a-Cre mice. AAV-iCre-2A-Venus or AAV-GFP (10–15 nl) was injected bilaterally into the SPZ of $Vgat^{lox/lox}$ mice. AAV-DIO-hM3Dq-mCherry (15 nl) was injected bilaterally into the VMH of *Pacap*-IRES-Cre mice. AAV8-DIO-synaptophysin-mCherry (10 nl) was injected unilaterally into the VMH of *Pacap*-IRES-Cre mice. To allow time for AAV expression, all mice were given at least 4 weeks before experiments.

Immediately following brain injections, $Vgat^{lox/lox}$ mice used in LMA and Tb recordings were implanted IP with biotelemetry transmitters (Data Sciences International, St. Paul, MN). Incisions were sutured and treated with topical antibiotic, and all mice received Meloxicam, an analgesic, for 48 h during recovery.

Resident-intruder paradigm

All "resident" mice ($Vgat^{lox/lox}$, C57BL6/J, *Vgat*-IRES-Cre, or *Pacap*-IRES-Cre) were sexually experienced adult males (4–6 months old at testing), singly housed and isolated from other males for at least 1 month, which produces a territorially aggressive phenotype. For behavioral tests we pre-adapted resident mice to clear cylindrical home containers (diameter, 20 cm; height, 25 cm) for at least 5 days. All residents were maintained in these home containers inside light-tight isolation chambers under a 12:12 light-dark (LD) cycle with lights on at 800 (zeitgeber time 0, ZT0). Chambers provided ventilation, ambient temperature of 22±2°C, and visual isolation from other mice. Mice received food (Lab Diet) and water *ad libitum*. Ambient lighting was provided by a white-light LED matrix, containing 18 single LEDs (light peak 490/540nm) using a phosphor layer (Yttrium Aluminum Garnet) on the surface of a blue (Gallium Nitride) chip (The LED Light, Inc.). For each test, residents were moved in their home containers to an adjacent testing room illuminated with red light (GE lighting, Red LED, A15, 620–640 nm), which does not alter circadian phase nor disrupt affective behaviors in nocturnal rodents[47], and given 5 min to acclimate. A male group-housed and sexually naïve "intruder" mouse (C57BL6/J), maintained on the same LD cycle in a separate chamber, was introduced into the resident's home container and behavioral interactions were video recorded for 10 min using 2 cameras from different lateral angles. No other mice were in the testing room during each test. Residents and intruders were always novel to one another and were of similar ages and weights.

We tested these mice under red light conditions, instead of under normal room lighting or only in the dark, in order to maintain the same level of visual cues across all time points. For instance, had half of our behavioral tests been performed in the light (at ZT1 and ZT7), resident mice would have had additional visual cues to aide them in attacking the intruder. On the other hand, had we instead put mice into a lighted environment during their normal dark phase (at ZT13 and ZT19), we might have actually induced sleep/inactivity (a phenomenon called negative masking) since mice are nocturnal, which would not have been conducive for measuring aggression. We do not believe that taking these mice out of a lighted environment and testing them under only red light biased our observed day-night (ZT1 vs ZT13, Fig. 1b–d) differences in aggression, because we saw similar temporal differences in attack behavior between CT1 and CT13 (Fig. S3) in our control mice that had been housed in constant darkness and then moved to red light conditions for testing in free running conditions (see below).

Littermate *Vgat*$^{lox/lox}$ mice (n=40) injected with AAV-iCre-2A-Venus or AAV-GFP into the SPZ were tested at 1 of 4 different time points: ZT1 (between 845–930), ZT7 (between 1445–1530), ZT13 (between 2045–2145), ZT19 (245–330). The order of time points was counter-balanced across all residents using a Latin square design. Following each test, home containers were changed and mice received 3–5 days before being tested again at the next time point until all 4 trials were completed. Mice were randomly assigned to experimental/control groups, and to which order they were tested.

Littermate *Vgat*-IRES-Cre mice (n=23) injected with AAV-FLEX-hGlyR-mCherry into the SPZ received either IVM (5 mg/kg in propylene glycol) or VEH, administered via IP injection at ZT1 or ZT13. Because IVM has a long half-life and minor off-target effects (drowsiness) that are no longer present after 24 h[48], we tested these mice using the same resident-intruder assay, as described above, at ZT1 or ZT13, respectively, on the following day. We allowed two weeks following each test to ensure drug clearance and then mice were injected with the other compound (IVM or VEH) and tested again 24 h later, serving as within-animal controls. Half of each group of mice received IVM first and half received VEH first, with mice being randomly assigned to each group. As an additional control for the phase-dependent effects of IVM, we tested an additional group of *Vgat*-IRES-Cre mice (n=10) injected with ChR2 into the SPZ (which does not respond to IVM) at ZT1 using the same methods described above.

Littermate *Pacap*-IRES-Cre mice (n=6) injected with AAV-DIO-hM3Dq-mCherry into the VMH received CNO (1 mg/kg in saline) or VEH, administered IP, 1h before being tested with resident-intruder assays at ZT1 as described above. Mice received 3–5 days to allow for drug clearance and were then injected with the other compound and tested again, serving as within-animal controls. Half of these mice received CNO first and half received VEH first, with mice being randomly assigned to each group. Previous studies have shown that CNO has no effect on aggressive behavior in either WT C57BL6 mice or control mice injected with an AAV not containing hM3Dq[49–51].

Littermate intact C57BL6/J (n=15) were used to assess rhythms of aggression propensity under free running conditons (constant darkness, DD). Mice were put into DD, extending

from the end of their normal dark period, for 2 full days and then tested at 1 of 4 time points: CT1 (between 845–930), CT11 (between 1845–1930), CT13 (between 2045–2145), or CT23 (between 645–730). Following each test, home containers were changed and mice were put back into LD for at least 3 days to reentrain, before being put back into DD for 2 full days and tested again at the next time point until all 4 trials were completed (6–8 days between each test). The order of tests for each mouse was counterbalanced using a Latin square design, with mice randomly assigned to each order. Although we would expect the internal phase of each mouse to drift in DD due to its period not being exactly 24 h, our data for average period length in DD (Table 1) from intact mice on a C57BL6 background would suggest an average drift of only about 15 min across 3 days [using the equation: (24 h – period length)* 60 min * 3 days]. Intruders used in these experiments were maintained on their normal LD schedule.

Recorded videos of resident-intruder tests were manually scored blind to the condition of each resident mouse and the time of day of the test. Videos were sequenced and the total time each resident spent engaged in attack behavior (including biting, chasing, lunging, wrestling, and boxing) was quantified on a frame-by-frame basis using the "Behavior Annotator" Matlab script developed by researchers at the California Institute of Technology (http://www.vision.caltech.edu/Video_Datasets/CRIM13/CRIM13/Main.html)[12,52]. The resident's total number of attack bouts and the latency to its first attack were also calculated. Behaviors of intruders, which did not display attack behavior, were not scored.

LMA and Tb rhythm recordings

A subset of littermate *Vgat*$^{lox/lox}$ mice (n=16), injected with AAV-iCre-2A-Venus or AAV-GFP into SPZ, also underwent Tb and LMA telemetry recordings at least 2 weeks after completion of all resident-intruder tests. Mice were individually housed in standard plastic cages inside isolation chambers as described above with *ad libitum* food and water. Cages were placed atop telemetry receivers interfaced to a microcomputer data acquisition system (Data Sciences International, New Brighton, MN, USA). Tb values were recorded at 5-min intervals, and LMA data were collected in 5-min bins. Cages were changed every 2 weeks and health checks were performed daily by real-time data analysis. We collected at least 10 days of LMA and Tb data under a 12:12 light-dark (LD) conditions, and at least 3 weeks in constant darkness (DD).

Day-night plasma corticosterone

A subset of littermate *Vgat*$^{lox/lox}$ mice (n=11), injected with AAV-iCre-2A-Venus or AAV-GFP into the SPZ and tested for aggression as described above, also underwent assessment of day-night plasma corticosterone levels. Mice were housed in standard laboratory cages with *ad libitum* food and water, and maintained undisturbed in isolation chambers as described above for at least 2 weeks under LD conditions. Blood was collected via tail snip at ZT1 or ZT13 and again 12h later (half underwent collection at ZT1 first and half at ZT13 first, with mice randomly assigned to each group). Tail blood collection and plasma corticosterone levels assays were as previous described[53]. About 10 μl of blood was collected in EDTA-coated microvette tubes within 60 s after touching the cage. Samples were centrifuged and 4 μl plasma was collected and diluted in 200 μl of steroid diluent.

Plasma corticosterone was determined using ^{125}I radioimmunoassay kit from MP Biomedicals. All samples were analyzed in duplicate in the same assay to avoid interassay variability.

Histology and immunohistochemistry

Deeply anesthetized mice were transcardially perfused with saline and 1:10 formalin. Brains were removed, postfixed, cryoprotected in sucrose solution until sinking, then cut into 30 μm coronal sections using a freezing microtome. Sections were washed in phosphate buffered saline (PBS), and incubated in primary AVP, VIP, hrGFP, Esr1, GFP, Cre, dsRed, CTb, or c-Fos antiserum diluted in PBS containing 0.3% Triton X-100 and 0.2% sodium azide overnight at room temperature. The AVP antibody (1:20K, Peninsula, cat#T-5048) was a guinea pig polyclonal raised against synthetic AVP (H-Cys-Tyr-Phe-Gln-Asn-Cys-Pro-Arg-Gly-NH_2). The VIP (1:10K, ImmunoStar, cat#20077) antibody was a rabbit polyclonal raised against porcine VIP conjugated to bovine thyroglobulin. The hrGFP (1:20K, Stratagene, cat#240142) antibody was a rabbit polyclonal raised against full-length recombinant hrGFP from *E. coli*. The Esr1 (1:3K, Millipore, cat#06-935) antibody used was a rabbit polyclonal raised against rat ERα (TYYIPPEAEGFPNTI). The GFP (1:20K, Invitrogen, cat#A-6455) antibody used was a rabbit polyclonal raised against 27kD GFP isolated from jellyfish *Aequorea victoria*. The Cre (1:5K, Novagen, cat#69050) antibody used was a rabbit polyclonal raised against bacteriophage P1 Cre Recombinase (35 kD). The dsRed (1:10K, Clontech, cat#632496) antibody was a rabbit polyclonal raised against DsRed-Express, variant of *Dicosoma* sp. red fluorescent protein. The CTb antibody (1:10K, List Biological, cat#703) was a goat polyclonal raised against choleragenoid. The c-Fos antibody (1:20K, ~55kD, Oncogene, cat#Ab5,) was a rabbit polyclonal raised against residues 4–17 human cFos. Additional validation details are available from the manufacturer for each antibody used.

Sections were washed in PBS and incubated in biotinylated secondary antiserum (against appropriate species, 1:500) in PBS containing 0.3% Triton X-100 for 1 h, washed in PBS and incubated in ABC reagents for 1 h. Sections were washed and incubated in a solution of 0.06% 3,3-diaminobenzidine tetrahydrochloride (DAB, Sigma) and 0.02% H_2O_2. Nickel-Cobalt solution was added to produce black byproduct for Cre, Esr1, and cFos labeling. For fluorescent immunohistochemistry (AVP and VIP, or CTb and cFos), sections were washed, incubated for 1 h in fluorescently conjugated secondary antisera (Alexa Fluor 488 anti-Rabbit, 1:500, for VIP and cFos; Alexa Fluor 568 anti-goat, 1:500, for CTb) or biotinylated secondary as above followed by washes and 1h incubation in fluorescently conjugated streptavidin (Alexa Fluor 568, 1:1K, for AVP). For controls, we verified that hrGFP, GFP, Cre, and CTb antibodies did not label cells in uninjected animals, that cFos antibody labeled typical patterns in unstimulated animals, and that AVP, VIP, and Esr1 antibodies labeled typical patterns in PV, SCN, and VMH, respectively[23,54,55].

Cell Counting

All cell counts were analyzed blind to the time of day of perfusion and the condition of each animal. For quantification of day-night differences in Fos expression, adult male *Vgat*-IRES-Cre mice, housed on a 12:12 LD cycle in chambers as described above, were perfused 90

min after ZT1 or ZT13 (n=9 per group). Bilateral images of the SPZ from sections immunostained for cFos were imported into ImageJ (NIH) and labeled neurons were counted in the last 2 sections containing the dSPZ using the Cell Counter plugin.

For quantification of differences of cFos expression following chemogenetic inhibition, a subset of *Vgat*-IRES-Cre injected with AAV-FLEX-hGlyR-mCherry into the SPZ and tested for aggression, as described above, were given IVM (n=3) or VEH (n=3) at ZT1, and then perfused 90 min after ZT1 on the following day. These mice were housed on a 12:12 LD cycle in chambers as described above, and were given at least 2 weeks after aggression testing before these perfusions. Unilateral images of the SPZ from sections immunostained for dsRed and cFos were imported into ImageJ. Double-labeled neurons were counted in last 2 sections containing the dSPZ sections using the Cell Counter plugin. An Abercrombie correction was applied to all cell counts[56].

Heat map generation

Each experimental mouse was given an aggression score based on the magnitude of its total time attacking at ZT1 compared to the control mean at this time. Each injection site showing the extent of transduced neurons [identified using immunolabeling against Cre ($Vgat^{lox/lox}$ mice) or dsRed (*Vgat*-IRES-Cre mice)] was digitally projected onto representative templates at three rostral→caudal levels throughout the anterior hypothalamus, constructed using immunolabeling against VIP and AVP (to better delineate the SCN and PV). Each mouse's injection site was weighted by its aggression score, and weighted sites for all mice were overlaid. Using a custom script (www.python.org, see Supplementary Software) the aggression score was summed over the group (pixel-by-pixel over each overlaid image), and heat maps were created demarcating brain regions most associated with increased aggression at ZT1, as previously described[57].

Digoxigenin (DIG)-labeled RNA Probe In Situ Hybridization

Sections were cut in RNAse-free conditions, preserved in RNAlater® RNA Stabilization Solution, and frozen until use. Sections were washed in RNAse free PBS containing diethylpyrocarbonate (DEPC) then incubated in hybridization buffer for 1 h at 53°C. VGAT probe was denatured at 80°C for 10 min then incubated in the hybridization buffer overnight at 53°C. Sections were successively washed in 2× standard saline citrate (SSC) with 50% formamide solution and in 1× SSC 50% with formamide solution, both at 53°C. After tris buffered saline (TBS, pH 7.5) washes, sections were incubated in 1% blocking reagent (Roche Applied Science, Penzberg, Germany) for 30 min, then incubated overnight in peroxidase conjugated DIG antibody (1:500, Roche Applied Science, Penzberg, Germany). Following TBS washes, sections were reacted with Tyramide signal amplification (TSA) Cy3 (1:50, Perkin Elmer, Waltham, MA) for 30 min. VGAT probes were produced by Dr. Shigefumi Yokota, University School of Medicine, Japan.

Statistical analyses

All data were imported into Prism 7 (Graphpad) and normality was assessed using D'Agostino-Pearson and Kolmogorov-Smirnov tests, to verify the appropriateness of the following statistical analyses. For $Vgat^{lox/lox}$ mice, aggression data scored during resident

intruder testing were compared across time and between SPZ conditions using two-way repeated measures ANOVA, with Sidak tests for multiple comparisons serving as *post hoc* analyses. Sample sizes were not predetermined using formal statistical tests for *Vgat*$^{lox/lox}$ mice, however, *post hoc* power calculations (G*Power software) using means and standard deviations from these analyses revealed this study was powered to detect respective effect sizes with >90% reliability. Because of natural variability within strains, not all mice show aggression, and we set a criteria before these experiments of at least one attack bout in at least half (50%) of all tests for inclusion in statistical analyses. Interestingly, only 2 *Vgat*-deleted mice failed to meet criteria for inclusion, whereas 6 intact controls failed. Overall, 80.0% of *Vgat*$^{lox/lox}$ mice met criteria for inclusion.

LMA and Tb data from *Vgat*$^{lox/lox}$ mice was first analyzed and plotted using Clocklab (Coulbourne Instruments, Natick, MA). For each mouse, we obtained LMA and Tb rhythm period (Chi-squared periodogram) and cosinor amplitude for the last 7 days in LD and the last 7 days in DD, and a two-way repeated measures ANOVA was used to compare between lighting and SPZ conditions with Sidak tests for multiple comparisons serving as *post hoc* analyses. We excluded data from 2 mice (1 SPZ *Vgat*-deleted and 1 intact SPZ GFP-injected) due to a computer failure during the DD recording. Mean LMA counts and Tb per hour were calculated for 7 days in LD and analyzed using two-way repeated measures ANOVA with Sidak tests for multiple comparisons as *post hoc* analyses. For comparing differences in day-night plasma corticosterone, two-way repeated measures ANOVA was used with Sidak tests for multiple comparisons as *post hoc* analyses.

Aggression data from *Vgat*-IRES-Cre mice was compared between IVM and VEH conditions using separate paired t tests for ZT1, ZT13, and ChR2-injected control groups. For *Pacap*-IRES-Cre mice, aggression data were compared between CNO and VEH conditions using paired t-tests. Sample sizes were not predetermined, however *post hoc* power calculations using means and standard deviations from *Vgat*-IRES-Cre, and *Pacap*-IRES-Cre, revealed we were powered to detect respective effect sizes with >90%, and 80%, reliability, respectively. For C57BL6/J mice, differences in aggression data between CT1 and CT13 were compared using planned comparsions (paired t tests). Sample size for C57BL6/J mice was predetermined (G*Power software) using the effect size, means and standard deviations of previously tested intact control mice on a C57BL6 background and a power level of 80%. We set the same criteria (at least one attack bout in 50% of test trials) for inclusion in these analyses. Overall, 72.7% of *Vgat*-IRES-Cre mice met criteria for inclusion (24 of 33), while 9 failed and were excluded. All 6 *Pacap*-IRES-Cre mice met criteria for inclusion. For C57BL6/J mice, 80% met criteria (12 of 15), while 3 failed and were excluded.

For cell counting in *Vgat*-IRES-Cre mice, differences in Fos expression were compared between ZT1 and ZT13 conditions and differences in dsRed/cFos-labeled cells were compared between IVM and VEH, conditions using unpaired t-tests. All data shown are means ± s.e.m. unless otherwise noted. For all tests, alpha was $P<0.05$.

Electrophysiology

Mice (9–12 weeks at testing) were deeply anesthetized, decapitated and brains quickly removed into ice-cold cutting solution consisting of (in mM): 72 sucrose, 83 NaCl, 2.5 KCl, 1 NaH_2PO4, 26 $NaHCO_3$, 22 glucose, 5 $MgCl_2$, 1 $CaCl_2$, oxygenated with 95% O_2/5% CO_2, measured osmolarity 310 – 320 mOsm/l. 300-μm-thick coronal sections were cut with Leica VT1000S vibratome and incubated in oxygenated cutting solution at 34 °C for 45 min. Slices were transferred to oxygenated aCSF (126 mM NaCl, 21.4 mM $NaHCO_3$, 2.5 mM KCl, 1.2 mM NaH_2PO_4, 1.2 mM $MgCl_2$, 2.4 mM $CaCl_2$, 10 mM glucose) and stored in the same solution at room temperature (20–24°C) for 60 min prior to recording. A single slice was placed in the recording chamber where it was continuously superfused at a rate of 3–4 ml per min with oxygenated aCSF. Neurons were visualized with an upright microscope (SliceScope, Scientifica) equipped with infrared-differential interference contrast and fluorescence optics. Borosilicate glass microelectrodes (5–7MΩ) were filled with internal solution.

Light-evoked EPSCs and IPSCs were recorded in whole-cell voltage-clamp mode, with membrane potential clamped at V_h=−70 mV. Light-evoked IPSCs were recorded using a CsCl-based internal solution consisting of (in mM): 140 CsCl, 1 BAPTA, 10 HEPES, 5 $MgCl_2$, 2 Mg-ATP, and 0.3 Na_2-GTP (pH 7.35 adjusted with NaOH; 295 mOsm·kg^{-1}). Light-evoked EPSCs were recorded using Cs^+-based internal solution consisting of (in mM): 135 $CsMeSO_3$, 10 HEPES, 1 EGTA, 4 $MgCl_2$, 4 Na_2-ATP, 0.4 Na_2-GTP, 10 Na_2-phosphocreatine (pH 7.3 adjusted with CsOH; 295 mOsm·kg^{-1}) in presence of bicuculline (10 μM).

The light-evoked EPSC/IPSC detection protocol consisted of four blue light pulses (473 nm wavelength, 0.5–5 msec) administered 1 s apart during the first 4 s of an 8-s sweep, repeated for a total of 30 sweeps. Evoked EPSCs/IPSCs with short latency (≤6ms) upon light stimulation were considered light-driven. As discussed by others, such currents are most likely monosynaptic[58]. Light-evoked IPSCs were recorded in presence of CNQX (10 μM) and D-AP5 (50 μM) to block polysynaptic glutamatergic excitation (Fig. 2). Due to the high local connectivity, light-driven monosynaptic EPSCs recorded from VMH neurons (Fig. 4), could be influenced by intra-nucleus polysynaptic glutamatergic excitation. It is noteworthy that this, however, does not change our overall finding that VMHc neurons are much more likely to connect to VMHvl neurons (13 out of 15 neurons; Fig. 4c) rather than VMHdm neurons (1 out 13 neurons; Fig. 4c). Number of animals used for CRACM experiments: SPZ^{GABA}→VMH, n=3; SCN^{VIP}→SPZ^{VMH}, n=2; $VMHc^{PACAP}$→VMHc, VMHdm or VMHvl, n=2 for each; SPZ→VMH^{Esr1}, n=4.

All recordings were made using Multiclamp 700B amplifier, and data were filtered at 2 kHz and digitized at 10 kHz. To photostimulate ChR2-positive fibers, a LED light source (473 nm) was used. Blue light was focused onto the back aperture of the microscope objective, producing wide-field exposure around recorded cell of 10–15mW per mm^2. Light power at specimen was measured using an optical power meter PM100D (Thorlabs). Light output was controlled by a programmable pulse stimulator, Master-8 (A.M.P.I.) and pClamp 10.2 software (Axon Instruments). All recordings were analyzed offline using Clampfit 10.

Data Availability

The data that support the findings of this study are presented within this paper or its supplementary materials or are available from the corresponding author upon reasonable request.

Code Availability

The custom code used for creating the weighted heat maps of our injection sites is available in Supplementary Software.

Supplementary Material

Refer to Web version on PubMed Central for supplementary material.

Acknowledgments

We thank Q. Ha, M. Thompson, S. Bandaru, C. Friedman, R. Thomas, and M. Ha for excellent technical assistance and C. Dulac for helpful comments during the early stages of this project. We thank J. Lynch (University of Queensland) for the hGlyR construct, and D. Anderson, X. Burgos-Artizzu, and P. Dollár (California Institute of Technology) for the Behavior Annotator MatLab script and code. This work was supported by the G. Harold and Leila Y. Mathers Foundation and the US National Institutes of Health (NIH) grants NS072337, NS085477, AG09975, and HL095491 to C.B.S., NS073613, NS092652, and NS103161 to P.M.F., and DK111401, DK075632, DK096010, DK089044, DK046200, and DK057521 to B.B.L. W.D.T. was supported by Alzheimer's Association grant AARF-16-443613 and NIH grants NS084582-01A1 and HL00701-15. N.L.M. was supported by CNPq (National Health Council for Scientific and Technological Development) grant 200881/2014-0, CAPES (Coordination for the Improvement of Higher Education Personnel).

References

1. Manfredini R, et al. Day-night variation in aggressive behavior among psychiatric inpatients. Chronobiol Int. 2001; 18:503–511. [PubMed: 11475419]
2. Bachman D, Rabins P. "Sundowning" and other temporally associated agitation states in dementia patients. Annu Rev Med. 2006; 57:499–511. DOI: 10.1146/annurev.med.57.071604.141451 [PubMed: 16409163]
3. Bronsard G, Bartolomei F. Rhythms, rhythmicity and aggression. J Physiol Paris. 2013; 107:327–334. DOI: 10.1016/j.jphysparis.2013.03.002 [PubMed: 23542545]
4. Jagannath A, Peirson SN, Foster RG. Sleep and circadian rhythm disruption in neuropsychiatric illness. Curr Opin Neurobiol. 2013; 23:888–894. DOI: 10.1016/j.conb.2013.03.008 [PubMed: 23618559]
5. Tordjman S, et al. Autism as a disorder of biological and behavioral rhythms: toward new therapeutic perspectives. Front Pediatr. 2015; 3:1. [PubMed: 25756039]
6. Miczek KA, Maxson SC, Fish EW, Faccidomo S. Aggressive behavioral phenotypes in mice. Behav Brain Res. 2001; 125:167–181. [PubMed: 11682108]
7. Miczek KA, et al. Neurobiology of escalated aggression and violence. J Neurosci. 2007; 27:11803–11806. DOI: 10.1523/JNEUROSCI.3500-07.2007 [PubMed: 17978016]
8. Nelson RJ, Trainor BC. Neural mechanisms of aggression. Nat Rev Neurosci. 2007; 8:536–546. DOI: 10.1038/nrn2174 [PubMed: 17585306]
9. Sternson SM. Hypothalamic survival circuits: blueprints for purposive behaviors. Neuron. 2013; 77:810–824. DOI: 10.1016/j.neuron.2013.02.018 [PubMed: 23473313]
10. Yang T, et al. Social Control of Hypothalamus-Mediated Male Aggression. Neuron. 2017; 95:955–970 e954. DOI: 10.1016/j.neuron.2017.06.046 [PubMed: 28757304]
11. Reppert SM, Weaver DR. Coordination of circadian timing in mammals. Nature. 2002; 418:935–941. DOI: 10.1038/nature00965 [PubMed: 12198538]

12. Lin D, et al. Functional identification of an aggression locus in the mouse hypothalamus. Nature. 2011; 470:221–226. DOI: 10.1038/nature09736 [PubMed: 21307935]
13. Yang CF, et al. Sexually dimorphic neurons in the ventromedial hypothalamus govern mating in both sexes and aggression in males. Cell. 2013; 153:896–909. DOI: 10.1016/j.cell.2013.04.017 [PubMed: 23663785]
14. Lee H, et al. Scalable control of mounting and attack by Esr1+ neurons in the ventromedial hypothalamus. Nature. 2014; 509:627–632. DOI: 10.1038/nature13169 [PubMed: 24739975]
15. Falkner AL, Grosenick L, Davidson TJ, Deisseroth K, Lin D. Hypothalamic control of male aggression-seeking behavior. Nat Neurosci. 2016; 19:596–604. DOI: 10.1038/nn.4264 [PubMed: 26950005]
16. Welsh DK, Logothetis DE, Meister M, Reppert SM. Individual neurons dissociated from rat suprachiasmatic nucleus express independently phased circadian firing rhythms. Neuron. 1995; 14:697–706. [PubMed: 7718233]
17. Jin X, et al. A molecular mechanism regulating rhythmic output from the suprachiasmatic circadian clock. Cell. 1999; 96:57–68. [PubMed: 9989497]
18. Gall AJ, Todd WD, Blumberg MS. Development of SCN connectivity and the circadian control of arousal: a diminishing role for humoral factors? PLoS One. 2012; 7:e45338. [PubMed: 23028945]
19. Saper CB. The central circadian timing system. Curr Opin Neurobiol. 2013; 23:747–751. DOI: 10.1016/j.conb.2013.04.004 [PubMed: 23706187]
20. Watts AG, Swanson LW, Sanchez-Watts G. Efferent projections of the suprachiasmatic nucleus: I. Studies using anterograde transport of Phaseolus vulgaris leucoagglutinin in the rat. J Comp Neurol. 1987; 258:204–229. DOI: 10.1002/cne.902580204 [PubMed: 3294923]
21. Watts AG, Swanson LW. Efferent projections of the suprachiasmatic nucleus: II. Studies using retrograde transport of fluorescent dyes and simultaneous peptide immunohistochemistry in the rat. J Comp Neurol. 1987; 258:230–252. DOI: 10.1002/cne.902580205 [PubMed: 2438309]
22. Lu J, et al. Contrasting effects of ibotenate lesions of the paraventricular nucleus and subparaventricular zone on sleep-wake cycle and temperature regulation. J Neurosci. 2001; 21:4864–4874. [PubMed: 11425913]
23. Vujovic N, Gooley JJ, Jhou TC, Saper CB. Projections from the subparaventricular zone define four channels of output from the circadian timing system. J Comp Neurol. 2015; 523:2714–2737. DOI: 10.1002/cne.23812 [PubMed: 26010698]
24. Tong Q, Ye CP, Jones JE, Elmquist JK, Lowell BB. Synaptic release of GABA by AgRP neurons is required for normal regulation of energy balance. Nat Neurosci. 2008; 11:998–1000. DOI: 10.1038/nn.2167 [PubMed: 19160495]
25. Kaur S, et al. Glutamatergic signaling from the parabrachial nucleus plays a critical role in hypercapnic arousal. J Neurosci. 2013; 33:7627–7640. DOI: 10.1523/JNEUROSCI.0173-13.2013 [PubMed: 23637157]
26. Engeland WC, Arnhold MM. Neural circuitry in the regulation of adrenal corticosterone rhythmicity. Endocrine. 2005; 28:325–332. DOI: 10.1385/ENDO:28:3:325 [PubMed: 16388123]
27. Vong L, et al. Leptin action on GABAergic neurons prevents obesity and reduces inhibitory tone to POMC neurons. Neuron. 2011; 71:142–154. DOI: 10.1016/j.neuron.2011.05.028 [PubMed: 21745644]
28. Chou TC, et al. Critical role of dorsomedial hypothalamic nucleus in a wide range of behavioral circadian rhythms. J Neurosci. 2003; 23:10691–10702. [PubMed: 14627654]
29. Krashes MJ, et al. An excitatory paraventricular nucleus to AgRP neuron circuit that drives hunger. Nature. 2014; 507:238–242. DOI: 10.1038/nature12956 [PubMed: 24487620]
30. Anaclet C, et al. The GABAergic parafacial zone is a medullary slow wave sleep-promoting center. Nat Neurosci. 2014; 17:1217–1224. DOI: 10.1038/nn.3789 [PubMed: 25129078]
31. Fan J, et al. Vasoactive intestinal polypeptide (VIP)-expressing neurons in the suprachiasmatic nucleus provide sparse GABAergic outputs to local neurons with circadian regulation occurring distal to the opening of postsynaptic GABAA ionotropic receptors. J Neurosci. 2015; 35:1905–1920. DOI: 10.1523/JNEUROSCI.2661-14.2015 [PubMed: 25653351]

32. Lynagh T, Lynch JW. An improved ivermectin-activated chloride channel receptor for inhibiting electrical activity in defined neuronal populations. J Biol Chem. 2010; 285:14890–14897. DOI: 10.1074/jbc.M110.107789 [PubMed: 20308070]
33. Berridge KC. Motivation concepts in behavioral neuroscience. Physiol Behav. 2004; 81:179–209. DOI: 10.1016/j.physbeh.2004.02.004 [PubMed: 15159167]
34. Kennedy A, et al. Internal States and Behavioral Decision-Making: Toward an Integration of Emotion and Cognition. Cold Spring Harb Symp Quant Biol. 2014; 79:199–210. DOI: 10.1101/sqb.2014.79.024984 [PubMed: 25948637]
35. LeDoux J. Rethinking the emotional brain. Neuron. 2012; 73:653–676. DOI: 10.1016/j.neuron.2012.02.004 [PubMed: 22365542]
36. Silva BA, et al. Independent hypothalamic circuits for social and predator fear. Nat Neurosci. 2013; 16:1731–1733. DOI: 10.1038/nn.3573 [PubMed: 24212674]
37. Kunwar PS, et al. Ventromedial hypothalamic neurons control a defensive emotion state. Elife. 2015; 4
38. Bilu C, Kronfeld-Schor N. Effects of circadian phase and melatonin injection on anxiety-like behavior in nocturnal and diurnal rodents. Chronobiol Int. 2013; 30:828–836. DOI: 10.3109/07420528.2013.773439 [PubMed: 23750894]
39. Albrecht A, Stork O. Circadian Rhythms in Fear Conditioning: An Overview of Behavioral, Brain System, and Molecular Interactions. Neural Plast. 2017; 2017:3750307. [PubMed: 28698810]
40. Nakamura W, et al. In vivo monitoring of circadian timing in freely moving mice. Curr Biol. 2008; 18:381–385. DOI: 10.1016/j.cub.2008.02.024 [PubMed: 18334203]
41. Todd WD, Gall AJ, Weiner JA, Blumberg MS. Distinct retinohypothalamic innervation patterns predict the developmental emergence of species-typical circadian phase preference in nocturnal Norway rats and diurnal nile grass rats. J Comp Neurol. 2012; 520:3277–3292. DOI: 10.1002/cne.23098 [PubMed: 22431036]
42. Hermes ML, Kolaj M, Doroshenko P, Coderre E, Renaud LP. Effects of VPAC2 receptor activation on membrane excitability and GABAergic transmission in subparaventricular zone neurons targeted by suprachiasmatic nucleus. J Neurophysiol. 2009; 102:1834–1842. DOI: 10.1152/jn.91261.2008 [PubMed: 19571188]
43. Khachiyants N, Trinkle D, Son SJ, Kim KY. Sundown syndrome in persons with dementia: an update. Psychiatry Investig. 2011; 8:275–287. DOI: 10.4306/pi.2011.8.4.275
44. Bedrosian TA, Nelson RJ. Sundowning syndrome in aging and dementia: research in mouse models. Exp Neurol. 2013; 243:67–73. DOI: 10.1016/j.expneurol.2012.05.005 [PubMed: 22627081]
45. Canevelli M, et al. Sundowning in Dementia: Clinical Relevance, Pathophysiological Determinants, and Therapeutic Approaches. Front Med (Lausanne). 2016; 3:73. [PubMed: 28083535]
46. Hope T, Keene J, Gedling K, Fairburn CG, Jacoby R. Predictors of institutionalization for people with dementia living at home with a carer. Int J Geriatr Psychiatry. 1998; 13:682–690. [PubMed: 9818303]
47. Bedrosian TA, et al. Nocturnal light exposure impairs affective responses in a wavelength-dependent manner. J Neurosci. 2013; 33:13081–13087. DOI: 10.1523/JNEUROSCI.5734-12.2013 [PubMed: 23926261]
48. Oishi Y, et al. Role of the medial prefrontal cortex in cataplexy. J Neurosci. 2013; 33:9743–9751. DOI: 10.1523/JNEUROSCI.0499-13.2013 [PubMed: 23739971]
49. Hattori T, et al. Self-Exposure to the Male Pheromone ESP1 Enhances Male Aggressiveness in Mice. Curr Biol. 2016; 26:1229–1234. DOI: 10.1016/j.cub.2016.03.029 [PubMed: 27151664]
50. Padilla SL, et al. Agouti-related peptide neural circuits mediate adaptive behaviors in the starved state. Nat Neurosci. 2016; 19:734–741. DOI: 10.1038/nn.4274 [PubMed: 27019015]
51. Hashikawa K, et al. Esr1(+) cells in the ventromedial hypothalamus control female aggression. Nat Neurosci. 2017; 20:1580–1590. DOI: 10.1038/nn.4644 [PubMed: 28920934]
52. Burgos-Artizzu, XP., Dollar, P., Lin, D., Anderson, DJ., Perona, P. IEEE Conference on Computer Vision and Pattern Recognition. Providence; Rhode Island: 2012.

53. Zhang R, et al. Loss of hypothalamic corticotropin-releasing hormone markedly reduces anxiety behaviors in mice. Mol Psychiatry. 2016

54. Pei H, Sutton AK, Burnett KH, Fuller PM, Olson DP. AVP neurons in the paraventricular nucleus of the hypothalamus regulate feeding. Mol Metab. 2014; 3:209–215. DOI: 10.1016/j.molmet.2013.12.006 [PubMed: 24634830]

55. Cheong RY, Czieselsky K, Porteous R, Herbison AE. Expression of ESR1 in Glutamatergic and GABAergic Neurons Is Essential for Normal Puberty Onset, Estrogen Feedback, and Fertility in Female Mice. J Neurosci. 2015; 35:14533–14543. DOI: 10.1523/JNEUROSCI.1776-15.2015 [PubMed: 26511244]

56. Guillery RW. On counting and counting errors. J Comp Neurol. 2002; 447:1–7. DOI: 10.1002/cne.10221 [PubMed: 11967890]

57. Venner A, Anaclet C, Broadhurst RY, Saper CB, Fuller PM. A Novel Population of Wake-Promoting GABAergic Neurons in the Ventral Lateral Hypothalamus. Curr Biol. 2016; 26:2137–2143. DOI: 10.1016/j.cub.2016.05.078 [PubMed: 27426511]

58. Petreanu L, Huber D, Sobczyk A, Svoboda K. Channelrhodopsin-2-assisted circuit mapping of long-range callosal projections. Nat Neurosci. 2007; 10:663–668. DOI: 10.1038/nn1891 [PubMed: 17435752]

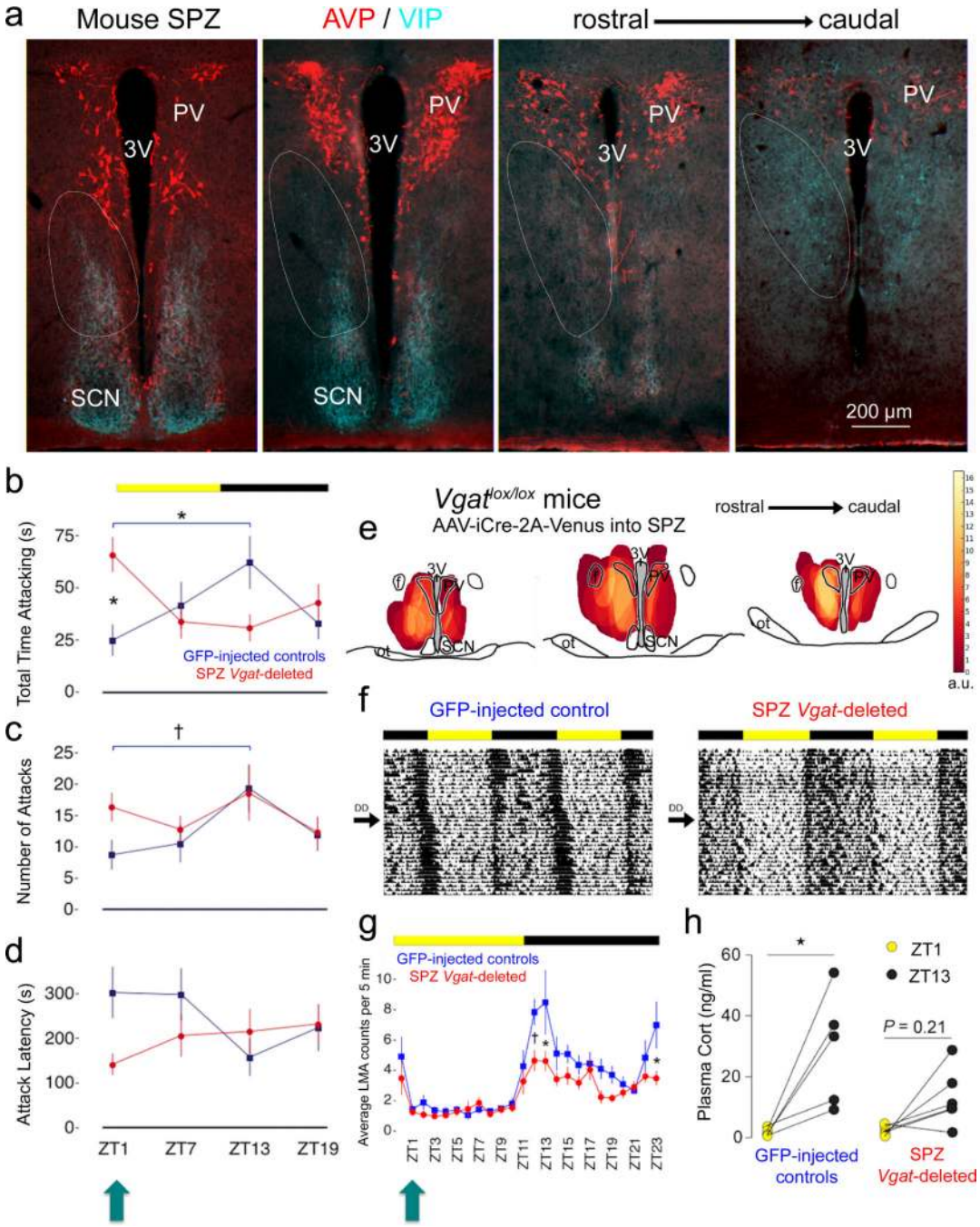

Figure 1. Aggression follows a daily rhythm in mice that is directly regulated by SPZ^{GABA} neurons

(a) Fluorescent immunohistochemistry for VIP (turquoise) and AVP (red) delineating the mouse SPZ (white ovals). Representative of 3 mice. 3V, third ventricle. (b) GFP-injected controls show a rhythm in aggression propensity with highest total time attacking at ZT13 and lowest at ZT1 [blue, n=16, two-way repeated measures ANOVA, interaction: $F_{(3,90)}$=7.63, *P*=.0001; *post hoc*: ZT13 vs ZT1 **P*=0.0067]. SPZ *Vgat*-deleted mice (red, n=16) show a disrupted rhythm with increased total time attacking at ZT1 (*post hoc*: deleted vs intact **P*=0.0055). Means ± s.e.m. (c) A similar rhythm in number of attacks was found

in controls [blue, n=12, two-way repeated measures ANOVA, main effect of time: $F_{(3,90)}$=6.25, *P*=0.0159; *post hoc*: ZT1 vs ZT13 †*P*=0.0244], which was lost in *Vgat*-deleted mice (red, n=16, *post hoc*: ZT1 vs ZT13 *P*=0.99). Means ± s.e.m. (d) Attack latency showed a significant interaction effect [two way repeated measures ANOVA, $F_{(3,90)}$=4.98, *P*=0.0362] with a trend towards differences at ZT1 and ZT13 in controls (blue, n=16, *post hoc*, ZT1 vs ZT13 *P*=0.0605), and towards decreased latency at ZT1 in *Vgat*-deleted mice (red, n=16, *post hoc:* deleted vs intact *P*=0.0683). Means ± s.e.m. (e) Heat map showing injection sites across *Vgat*-deleted mice (n=16), each weighted based on magnitude of difference from controls in total time attacking at ZT1. a.u., arbitrary units. ot, optic tract. f, fornix. (f) Double-plotted actograms of entrained (12:12 light-dark cycle, LD), and free-running (constant darkness, DD) LMA rhythms. (g) SPZ *Vgat*-deleted mice (red, n=8) exhibited decreased LMA during the dark period compared to controls (blue, n=8) [two-way repeated measures ANOVA, main effects of SPZ condition: $F_{(1,14)}$=11.34, P=0.0046, time: $F_{(23,322)}$=12.58, P=0.0001, interaction: $F_{(23,322)}$=1.61, P=0.0393, *post hoc:* ZT12 †*P*=0.0204, ZT13 **P*=0.0014, ZT23 **P*=0.0066]. Importantly, SPZ *Vgat*-deleted mice did *not* show increased LMA at ZT1 (turquoise arrow, *post hoc: P*=0.99). Means ± s.e.m. (h) SPZ *Vgat*-deleted mice (n=6) also showed lower day-night differences of plasma corticosterone compared to controls (n=5) [two-way repeated measures ANOVA, main effect of time: $F_{(1,9)}$=18.02, *P*=0.0022, *post hoc:* deleted ZT1 vs. ZT13 $^{n.s.}$*P*=0.21, intact ZT1 vs. ZT13 **P*=0.005]. Means ± s.e.m.

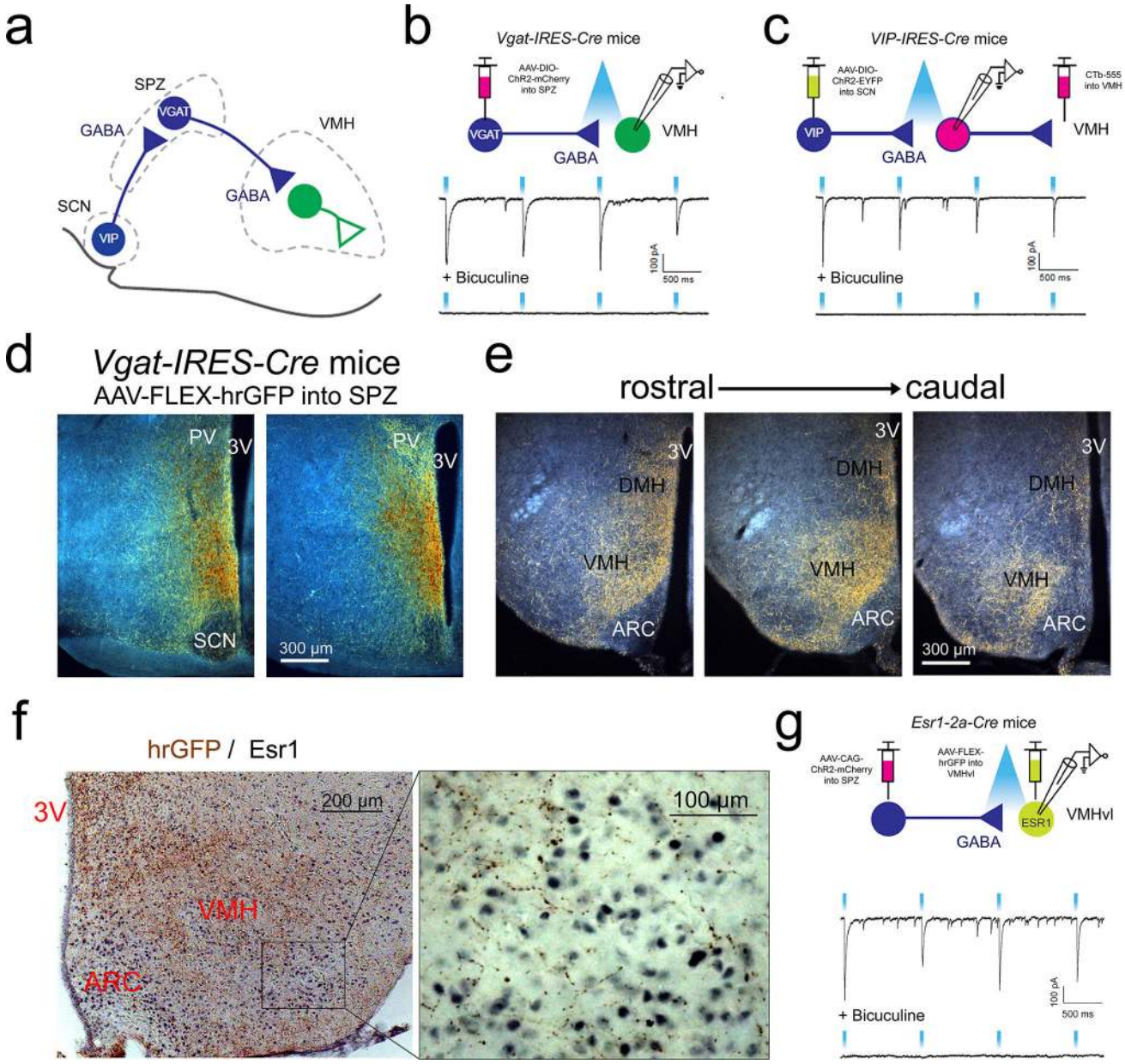

Figure 2. SPZ^{GABA} neurons project to and inhibit VMH neurons, and receive input from VIP neurons of the SCN

(a) A schematic drawing of the proposed SCN→SPZ→VMH neural circuit. (b) and (c) Top, schematics showing connections being tested. Bottom, representative traces of light-evoked IPSCs before and after bath application of bicuculline ($GABA_AR$ antagonist). (b) SPZ^{GABA} neurons in *Vgat*-IRES-Cre mice were transduced with AAV-DIO-ChR2-mCherry. Representative of 3 mice from multiple litters. (c) SCN^{VIP} neurons in Vip-IRES-Cre mice were transduced with AAV-DIO-ChR2-EYFP. SPZ$^{→VMH}$ neurons were labeled by CTb-555 injected into the VMH. Representative of 2 mice from different litters. (d) Darkfield photomicrograph of representative SPZ AAV-FLEX-hrGFP injection site in a Vgat-IRES-Cre mouse. Transduced neurons are orange/brown and fibers are yellow/gold. Representative of 4 mice. (e) Darkfield photomicrograph of representative hrGFP-labeled fibers (yellow/

gold) in the VMH and DMH in the same mouse as (d). Representative of 4 mice. ARC, arcuate nucleus. (f) Brightfield photomicrograph of representative hypothalamic section stained for hrGFP (brown) and estrogen receptor 1 (Esr1, black). Representative of 4 mice. (g) Top, schematic showing connections being tested. Bottom, representative traces of light-evoked IPSCs before and after bath application of bicuculline. In *Esr1*-2a-Cre mice, SPZ neurons were transduced by an injection of Cre-independent AAV-CAG-ChR2-mCherry and *Esr1*-expressing VMHvl neurons were labeled by an injection of AAV-FLEX-hrGFP. Representative of 4 mice from multiple litters.

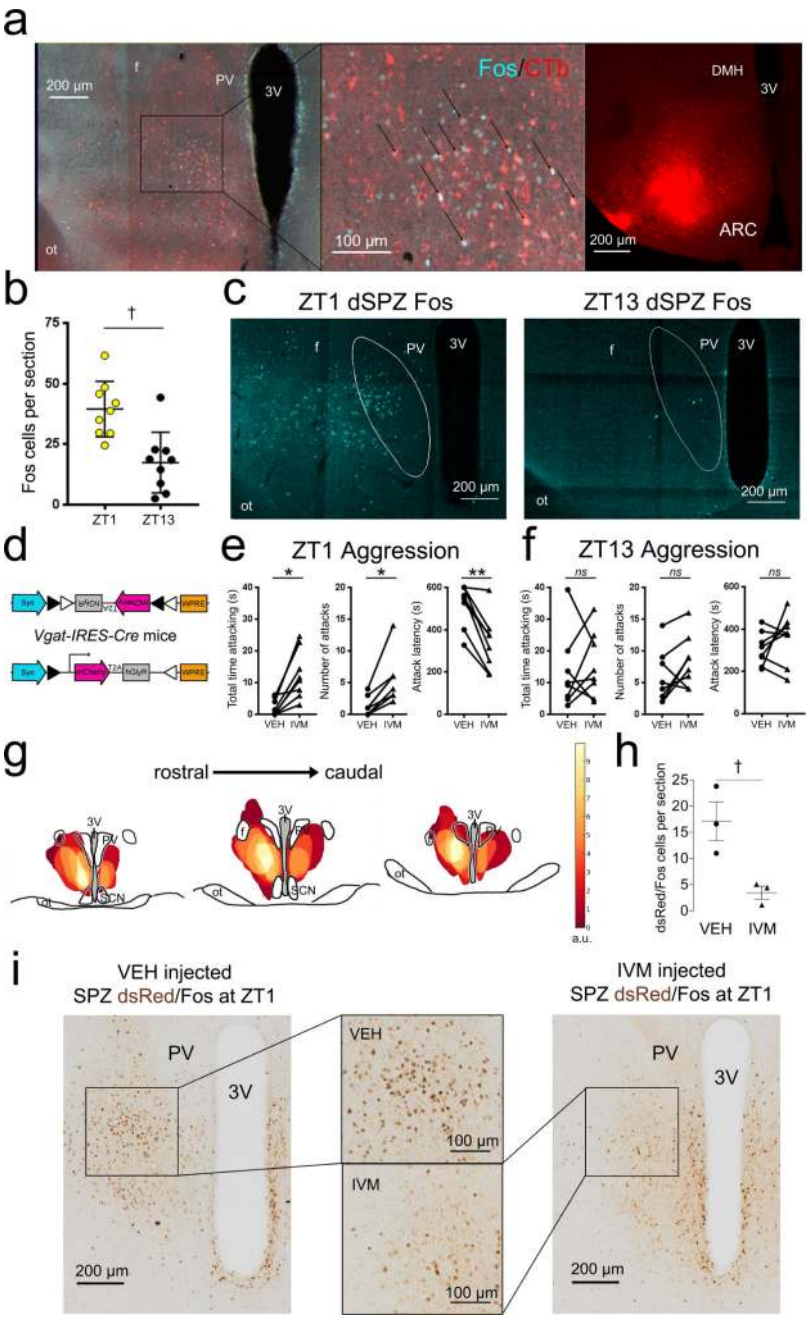

Figure 3. SPZ$^{\rightarrow VMH}$ neurons are more active at ZT1 than ZT13, and chemogenetic inhibition of SPZ^{GABA} transmission increases aggression at ZT1 but not ZT13

(a) Retrograde tracer CTb injected into the VMH (right) labeled neurons (red, left and center) in the dorsal SPZ (dSPZ) that also show Fos expression (a marker of neuronal activation, turquoise) at ZT1. Representative of 4 mice. (b) dSPZ neurons are significantly more active at ZT1 (n=9) compared to ZT13 (n=9) (unpaired t test, two-tailed, $t_{(16)}$=3.903: *P=0.0013). (c) Sections depicting differences in dSPZ cFos expression at ZT1 (left, representative of 9 mice) and ZT13 (right, representative of 9 mice). (d) Construct of AAV-FLEX-hGlyR-mCherry inhibitory vector, containing a FLEX cassette in reverse orientation and flanked by loxP sites. Cre-recombinase excises these sites and the cassette flips and

locks into the correct orientation, permitting expression of hGLYR-mCherry in cre+ cells. (e) At ZT1, *Vgat*-IRES-Cre mice (n=8) injected with AAV-FLEX-hGlyR-mCherry into the SPZ show increased total time attacking (left; paired t tests, two-tailed, $t_{(7)}$=4.404, **P*=0.0031), increased number of attacks (center; paired t test, two-tailed, $t_{(7)}$=4.615, **P*=0.0024), and decreased attack latency (right; paired t tests, two-tailed, $t_{(7)}$=5.686, ***P*s=0.0007), following administration of IVM compared to VEH. Means ± s.e.m. (f) In additional *Vgat*-IRES-Cre mice (n=8) injected with AAV-FLEX-hGlyR-mCherry into the SPZ, IVM administration did not significantly increase aggression propensity compared to VEH at ZT13 (paired t tests, two-tailed; time attacking, $t_{(7)}$=0.5467, ^{ns}P=0.6016; number of attacks, $t_{(7)}$=1.93, ^{ns}P=0.0949; attack latency, $t_{(7)}$=1.118, ^{ns}P=0.3005). Means ± s.e.m. (g) Heat map depicting overlapping injection sites within the SPZ, each weighted according to the magnitude of difference in total time attacking for the IVM condition compared to the mean VEH response. Arbitrary units. (h) *Vgat*-IRES-Cre mice injected with AAV-FLEX-hGlyR-mCherry into the SPZ were injected with IVM (n=3) or VEH (n=3) at ZT1 and then perfused 90 min after ZT1 on the following day. Mice receiving IVM showed significantly fewer dsRed-containing (marker for neurons injected with AAV-FLEX-hGlyR-mCherry, brown) neurons that expressed Fos (black) compared to mice receiving VEH (unpaired t test, two-tailed, $t_{(4)}$=3.497, $^{\dagger}P$=0.025). Means ± s.e.m. (i) Representative sections depicting decrease in dsRed/Fos double labeling at ZT1 in the dSPZ (center boxes) following IVM (right, representative of 3 mice) compared to VEH (left, representative of 3 mice) administration.

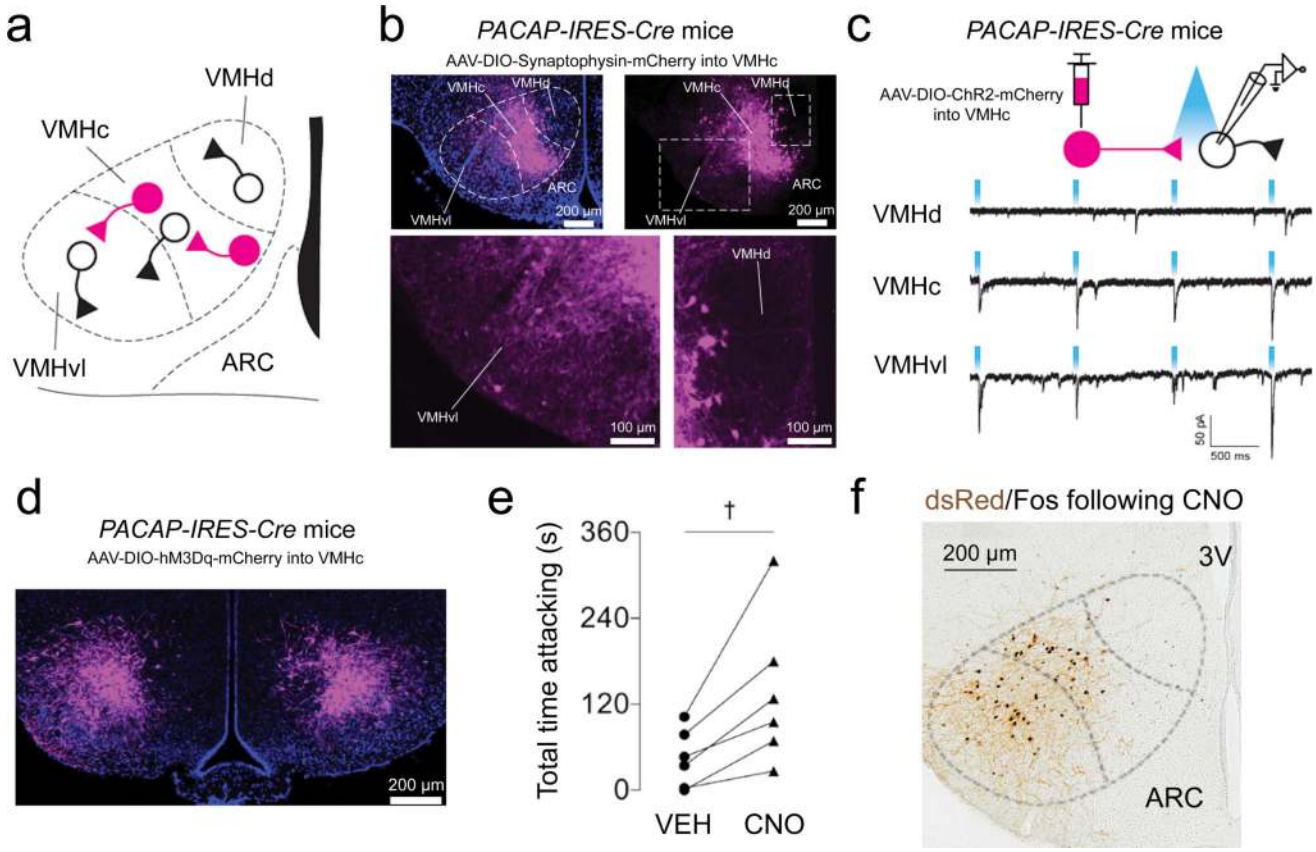

Figure 4. VMHc neurons strongly excite VMHvl neurons and drive behavioral aggression

(a) Schematic of VMH connectivity. (b) *Pacap*-IRES-Cre mice were injected with AAV-DIO-synaptophysin-mCherry, which expresses the synaptic vesicle protein, synaptophysin fused with mCherry in a cre-dependent fashion. Top, expression of AAV-DIO-synaptophysin-mCherry in $VMHc^{PACAP}$ neurons and $VMHc^{PACAP}$ terminals. Bottom, expression of AAV-DIO-synaptophysin-mCherry of $VMHc^{PACAP}$ terminals in the VMHvl (left box). Very few $VMHc^{PACAP}$ terminals were found in the VMHdm (right box). Representative of 3 mice. (c) Top, schematic shows connections being tested using CRACM. $VMHc^{PACAP}$ neurons in *Pacap*-IRES-Cre mice were transduced with AAV-DIO-ChR2-mCherry. Light-evoked EPSCs were detected in mCherry-negative neurons in the VMHc (representative of 2 mice from different litters) and VMHvl (representative of 2 mice from different litters), but not in the VMHdm (representative of 2 mice from different litters). (d) $VMHc^{PACAP}$ neurons in *Pacap*-IRES-Cre mice were bilaterally transduced with AAV-DIO-hM3Dq-mCherry. Representative of 6 mice. (e) CNO/hM3Dq-mediated stimulation of $VMHc^{PACAP}$ neurons in *Pacap*-IRES-Cre mice increased total time attacking (n=6, paired t test, two-tailed, $t_{(5)}=3.337$, $^{\dagger}P=0.0206$). Means ± s.e.m. (f) CNO administration 2 h before perfusion produced a robust Fos response in $VMHc^{PACAP}$ neurons expressing AAV-DIO-hM3Dq-mCherry (immunostained for dsRed) as well as in hM3Dq-negative VMHvl neurons. Representative of 3 mice.

Table 1

SPZ *Vgat* deletions disrupt entrained and free-running rhythms of LMA, but not Tb

SPZ *Vgat*-deleted mice (receiving AAV-iCre-2A-Venus) displayed decreased amplitude, but not period length (Tau), of LMA rhythms under entrained (LD, 12:12 light-dark cycle) and free-running (DD, constant darkness) conditions compared to intact AAV-GFP injected mice.

SPZ groups	LMA amplitude	LMA Tau	Tb amplitude	Tb Tau
AAV-iCre-2A-Venus (n=7)	(LD) 1.99±0.13 † (DD) 1.84±0.16 *	(LD) 24.00±0.12 (DD) 23.95±0.06	(LD) 0.52±0.02 (DD) 0.51±0.02	(LD) 23.83±0.00 (DD) 23.87±0.04
AAV-GFP (n=7)	(LD) 2.76±0.20 † (DD) 2.86±0.25 *	(LD) 23.93±0.12 (DD) 23.95±0.06	(LD) 0.58±0.03 (DD) 0.56±0.01	(LD) 23.83±0.00 (DD) 23.83±0.00

*, group difference in DD (P=0.002).

†, group difference in LD (P=0.0182). Tb rhythms were not affected by these *Vgat* deletions. Two-way repeated measures ANOVA followed by Sidak post hoc tests for multiple comparisons. Mean ± s.e.m.